

## Packing systematics and structural relationships of the new copper molybdate markascherite and related minerals

RICHARD M. THOMPSON,\* HEXIONG YANG, AND ROBERT T. DOWNS

Department of Geosciences, University of Arizona, 1040 E. 4th Street, Tucson, Arizona 85721, U.S.A.

### ABSTRACT

The structural relationships between the new mineral markascherite, ideally  $\text{Cu}_3(\text{MoO}_4)(\text{OH})_4$ , and the related minerals szenicsite, antlerite, deloryite, flinkite, retzian, and cahnite are analyzed using hypothetical ideal closest-packed equivalents. Markascherite and the first three related minerals are based on cubic closest-packing (CCP) of anions, flinkite is based on stacking sequence ABAC, and retzian and cahnite are based on hexagonal closest-packing (HCP). However, models that are more realistic than those based on CP can be constructed for retzian and cahnite using small but systematic alterations of CP monolayers. A regular pattern of slight dislocations of some of the spheres in the monolayers creates dodecahedral interstitial sites when the monolayers are stacked, a feature not seen in perfect CP.

The use of ideal crystals removes all distortion from polyhedra in closest-packed minerals, allowing for comparison of structural similarities and differences. CCP minerals can have up to four nonequivalent stacking directions. Corresponding stacking directions in the minerals of interest are identified and used to compare the layers of cation coordination polyhedra perpendicular to these zones or face poles (stacking directions are presented in both direct space and reciprocal space). Such layers are natural structural subunits and provide insight into the relationships among these minerals.

**Keywords:** Markascherite, szenicsite, antlerite, closest-packing, deloryite, flinkite, cahnite, retzian

### INTRODUCTION

Identifying the packing schemes of the anion arrangements of crystal structures is one of the fundamental tasks of building a comprehensive understanding of mineral systematics. Interest in the packing of spherical atoms as the basis of matter goes back at least to the late 16th century and the atomist Thomas Harriot (Hales 2000), who convinced the skeptical Kepler (1611) to investigate the problem of determining the densest possible arrangement of equal-sized spheres. The resulting Kepler Conjecture, stating that no packing of spheres can be denser than the face-centered cubic packing, remained unproven until the year 1998 (Hales 2000). In the late 19th century, Barlow (1883) began generating various packings and deriving the resulting symmetries, recognizing that many real crystal structures must be based on distortions of his idealized models. Early workers such as Pauling (1940) and Bragg et al. (1965) emphasized the importance of systematics such as packing schemes and coordination polyhedra, not only for their value as an intellectual framework, but also from practical necessity because they had to solve crystal structures by hand.

### CLOSE PACKING AND DISTORTION

Understanding structural relationships between minerals is important as it leads toward understanding the mechanisms of phase transformation and the ways that minerals adapt to varying

conditions. Unfortunately, it is not always obvious how minerals with related chemistries and/or structures should be oriented relative to each other for comparison. An examination of the anion skeleton can provide a starting point. It is natural to align stacking vectors in minerals that are based on closest-packing of anions to compare them.

In addition, hypothetical ideal equivalent crystals can be derived that have perfectly closest-packed arrangements of anions and regular cation-coordination polyhedra. All distortion can thereby be removed from the structures, enhancing visual analysis and clearly illustrating possible phase transition pathways. In particular, the layers formed by two CP oxygen monolayers and the cations between them are natural structural subunits, forming one layer of cation coordination octahedra, tetrahedra, or both. Comparing these subunits across different minerals is an insightful way to evaluate different crystal structures. This paper examines seven minerals using this approach. Where appropriate, possible transition pathways that have minimal cation diffusion distances are described.

We will use a parameter,  $U_{cp}$  (Thompson and Downs 2001), that expresses the degree of distortion of an arrangement of atoms from perfectly closest-packed to quantitatively compare the oxygen anion skeletons of markascherite and related CP minerals. In the CCP (HCP) case, it is the minimum mean-square displacement of 675 (677) corresponding anions contained in a spherical volume of space in the observed and ideal structures. The parameter is calculated by allowing the ideal structure to

\* E-mail: rmthomps@email.arizona.edu

translate, rotate, and isotropically expand or compress relative to the observed structure until the minimum value ( $U_{cp}$ ) is found. For the stacking sequence ABAC, we use a block of 672 anions. A value of zero for  $U_{cp}$  indicates an anion skeleton that is perfectly closest-packed, with distortion increasing as  $U_{cp}$  gets larger. A value of 1 indicates an oxygen arrangement that is extremely distorted.

CP minerals can be distorted from ideal by mismatches in cation size, uneven distributions of the strengths of electrostatic interactions, and other mechanisms. For example, Tait et al. (2011) analyzed the whitlockite-group minerals using  $U_{cp}$  and showed that the arrangement of the large, disk-shaped  $[M(TO_4)_6]^{16-}$  ligands form a distorted CCP arrangement, behaving much like the ligands consisting of single oxygen atoms in many other CCP minerals. The anionic units have ideal positional parameters but their flattened nature creates non-ideal axial ratios, resulting in extremely high values of distortion.

Yang et al. (2012) compared markascherite and related minerals, including the other known hydroxyl molybdates and some compounds of general chemical formula  $M_3(XO_4)(OH)_4$ , where  $M$  = divalent or trivalent cations and  $X$  = tetrahedrally coordinated  $Mo^{6+}$ ,  $S^{6+}$ ,  $Se^{6+}$ ,  $As^{5+}$ , or  $Si^{4+}$ . In this companion paper, we are interested in comparing the minerals from Yang et al. (2012) that are based on CP, but it is not always straightforward to distinguish CP from non-CP. Any closest-packed arrangement of spheres fills space with regular octahedra and tetrahedra, with each polyhedron defined by vertices at sphere centers. Cations in minerals with undistorted CP arrangements of anions are at or near the centers of such polyhedra, and are therefore either tetrahedrally or octahedrally coordinated. Hereafter, the terms “tetrahedra” and “octahedra” will generically refer to polyhedra when the context is such that it is irrelevant whether or not these polyhedra are occupied by cations or vacant. We will use “T” and “O” when referring to sites known to be occupied. Thus, for example, an “O double chain” is synonymous with a “double chain of octahedrally coordinated cations” and a “T site” is synonymous with a “tetrahedrally coordinated cation.” The tetrahedra in an ideal CP arrangement can be thought of as having a base perpendicular to the stacking direction and an apex pointing in the stacking direction. However, it is possible that distortion in a closest-packed arrangement of anions might allow for non-ideal coordination numbers and different orientations of the tetrahedra. For instance, diopside contains 8-coordinated calcium and yet is considered to be based on CCP (Downs 2003; Thompson and Downs 2008). Using in-house software and visual inspection, the following minerals from Yang et al. (2012) have been determined to be CP: markascherite, szenicsite, antlerite, deloryite, flinkite, retzian, and cahnite (see Table 1 for formulas). Note that Lima-de-Faria (2012) recently included antlerite in a list of CP minerals. Below we explore the relationships between these minerals.

## DISCUSSION

All closest-packed stacking sequences with the exception of CCP have a unique stacking direction perpendicular to the closest-packed monolayers. CCP has four equivalent stacking directions. In a face-centered cubic setting generated from an asymmetric unit with an atom at the origin using space group

$F\bar{4}3m$  or  $Fm\bar{3}m$ , closest-packed monolayers are stacked perpendicular to zones  $[111]$ ,  $[1\bar{1}\bar{1}]$ ,  $[\bar{1}\bar{1}1]$ , and  $[\bar{1}\bar{1}\bar{1}]$  (Fig. 1). In a mineral with an oxygen anion arrangement based on CCP, the stacking directions are determined by the setting chosen to describe the crystal. While the ideal anion packing may have four equivalent stacking directions, the cations in the structure may make one or more stacking directions nonequivalent.

Our analysis (Thompson and Downs 2001) determined that markascherite (Yang et al. 2012), szenicsite (Stoltz and Armbruster 1998), antlerite (Vilminot et al. 2003), and deloryite (Pushcharovsky et al. 1996) are based on CCP. Flinkite (Moore 1967) is based on the stacking sequence ABAC. The structures of retzian (Moore 1967) and cahnite (Prewitt and Buerger 1961) each contain an 8-coordinated cation, and therefore must be non-CP or quite distorted. Our investigation indicates that they are based on HCP, and the accommodation of the 8-coordinated cation in their structures is explored in depth in the Retzian and Cahnite subsections.

Table 1 contains the crystal structure data for the ideal equivalents of markascherite and its related CP minerals. Cell parameters are given in terms of the model oxygen radius,  $r$ . Values for  $r$  are provided that result in ideal crystals with volumes matching those of the observed minerals. Table 1 also lists the crystallographically nonequivalent stacking directions in each of the structures. Structures listed in Table 1 are ideal structures and as such have no errors associated with their cell and positional parameters, which are exact.  $U_{cp}$  is calculated with a minimizer that does not report errors. The value of the model oxygen radius,  $r$ , is arbitrarily chosen so that the model volume equals the reported value for the observed mineral to the reported precision.

### Szenicsite and antlerite

Szenicsite (Stoltz and Armbruster 1998) and antlerite (Vilminot et al. 2003) have closely related structures based on CCP of anions. In each structure, cations have divided the four equivalent CCP stacking directions into two pairs of equivalent stacking directions. Therefore, these minerals can be analyzed by examining two representative nonequivalent stacking directions and neglecting the other two. The corresponding stacking zones in the two minerals are  $[110]$  and  $[012]$  in szenicsite and  $[101]$  and  $[120]$  in antlerite, respectively. The rest of this subsection compares the corresponding zones  $[110]$  in szenicsite and  $[101]$  in antlerite, leaving examination of  $[012]$  and antlerite’s corresponding  $[120]$  for the szenicsite, antlerite, and markascherite subsection.

Along  $[110]$  in szenicsite ( $[101]$  in antlerite), the structures are built from two alternating layer types. Figure 2a shows a part of one of the layer types in an ideal structure. This layer type is composed solely of O sites and is hereafter referred to as the O layer. The O layer repeat unit consists of an O triple chain and two O single chains. In reality, the single chains are components of triple chains in the layers stacked along the equivalent stacking direction to  $[110]$ ,  $[1\bar{1}0]$  ( $[10\bar{1}]$  in antlerite).  $[1\bar{1}0]$  is angled at  $\cos^{-1}(1/3) = 70.53^\circ$  to  $[110]$ . The O layers are identical in szenicsite and antlerite.

The other layer type is composed of T and O sites in a 2:1 ratio and is hereafter referred to as the T layer. Figure 2b shows the difference between these two layers in ideal antlerite and

**TABLE 1.** Crystallographic and chemical information for ideal markascherite and related minerals parameterized in terms of the model oxygen radius,  $r$ 

Ideal mineral	Markascherite	Szenicsite	Antlerite	Deloryite	Flinkite 1	Flinkite 2	Retzian 1	Retzian 2
Formula	$\text{Cu}_3(\text{MoO}_4)(\text{OH})_4$	$\text{Cu}_3(\text{MoO}_4)(\text{OH})_4$	$\text{Cu}_3\text{SO}_4(\text{OH})_4$	$\text{Cu}_4(\text{UO}_2)\text{Mo}_2\text{O}_8(\text{OH})_6$	$\text{Mn}_3(\text{AsO}_4)(\text{OH})_4$		$\text{Mn}_2\text{Y}(\text{AsO}_4)(\text{OH})_4$	
Packing	CCP (ABC)	CCP (ABC)	CCP (ABC)	CCP (ABC)	ABAC	AA'B'B	HCP (AB)	$\text{A}_8\text{B}_8$
Stacking vectors D-space*	[301][105][143]	[012][110]	[101][120]	[304][1012][184]	[100]	[100]	[001]	[001]
Stacking vectors R-space	(100)(101)(121)	(011)(210)	(102)(110)	(100)(001)(421̄)	(100)	(100)	(001)	(001)
$U_{\text{cp}} \uparrow (\text{\AA}^2)$	0.23745	0.15660	0.25665	0.66316	1.08482	0.88032	0.75294	1.06406
$r (\text{\AA}) V_{\text{ideal}} = V_{\text{obs}}$	1.5361	1.5310	1.4972	1.5334	1.5370	1.5370	1.542	1.310
$V (\text{\AA}^3)$	$64\sqrt{2}r^3$	$128\sqrt{2}r^3$	$128\sqrt{2}r^3$	$128\sqrt{2}r^3$	$128\sqrt{2}r^3$	$128\sqrt{2}r^3$	$64\sqrt{2}r^3$	$6(3\sqrt{6+6}\sqrt{3} + 2\sqrt{2+4})r^3$
Space group	$P2_1/m$	$Pnnm$	$Pnma$	$C2/m$	$P2_1ma\ddagger$	$Pnma$	$Pban$	$P2/a$
$a$	$2\sqrt{11}r$	$8r$	$4\sqrt{2}r$	$8\sqrt{3}r$	$8\sqrt{6}r/3$	$8\sqrt{6}r/3$	$2\sqrt{3}r$	$3\sqrt{2}r$
$b$	$4r$	$4\sqrt{2}r$	$4r$	$4r$	$8r$	$8r$	$8r$	$(3\sqrt{6+2}\sqrt{2})r$
$c$	$2\sqrt{3}r$	$4r$	$8r$	$2\sqrt{3}r$	$2\sqrt{3}r$	$2\sqrt{3}r$	$4\sqrt{6}r/3$	$(2+\sqrt{2})r$
$\beta$	$\cos^{-1}(-1/\sqrt{33})$	90	90	$\cos^{-1}(-1/3)$	90	90	90	90
M1	[0, 3/4, 0]	[3/8, 1/4, 1/4]	[0, 1/4, 0]	[1/4, 0, 1/2]	[0, 0, 0]	[0, 0, 0]	[1/4, 9/16, 0]	[1/4, (55-2√3)/92, 0]
M1B							[1/4, 15/16, 0]	
M2	[0, 1/2, 1/2]	[1/2, 1/2, 1/2]	[1/4, 0, 1/8]	[1/4, 1/4, 0]	[0, 1/8, 1/2]	[0, 1/8, 1/2]	[1/4, 1/4, 0]	[1/4, 1/4, 0]
M3	[1/2, 1/2, 0]	[1/2, 1/2, 0]		[0, 0, 0]	[0, 7/8, 1/2]			
TA					[3/16, 3/4, 0]	[13/64, 3/4, 0]	[3/4, 1/4, 1/2]	[3/4, 1/4, 1/2]
TB	[5/16, 1/4, 7/16]	[1/8, 3/8, 0]	[1/8, 1/4, 3/8]	[13/32, 0, 3/8]	[5/16, 1/4, 2/3]	[13/64, 3/4, 0]		
O1	[1/8, 1/4, 3/8]	[1/2, 1/4, 0]	[1/4, 1/4, 1/4]	[1/16, 0, 1/4]	[1/8, 1/8, 1/6]	[1/8, 1/8, 1/6]	[5/12, 5/16, 1/4]	[7/12, (19+6√3)/92, 1-√2/2]
O2	[3/8, 1/4, 1/8]	[1/4, 1/4, 1/2]	[1/4, 1/4, 1/2]	[5/16, 0, 1/4]	[1/8, 0, 2/3]	[7/8, 1/8, 5/6]	[5/12, 13/16, 1/4]	[7/12, (55-2√3)/92, 1-√2/2]
O3	[3/8, 0, 5/8]	[3/8, 1/2, 1/4]	[0, 0, 3/8]	[7/16, 1/4, 1/4]	[1/8, 5/8, 1/6]	[7/8, 0, 1/3]	[5/12, 9/16, 1/4]	
O4	[1/8, 3/4, 3/8]	[1/4, 1/4, 0]	[1/4, 1/4, 0]	[7/16, 0, 3/4]	[1/8, 1/4, 2/3]	[1/8, 3/4, 2/3]	[5/12, 1/16, 1/4]	
O5	[3/8, 3/4, 1/8]	[1/8, 1/2, 1/4]	[3/4, 1/4, 3/4]	[3/16, 0, 3/4]	[1/8, 3/4, 2/3]	[1/8, 3/4, 2/3]		
O6	[1/8, 1/2, 7/8]	[0, 1/4, 0]	[0, 1/2, 1/8]	[3/16, 1/4, 1/4]	[3/8, 0, 0]			
O7					[3/8, 1/8, 1/2]			
O8					[3/8, 1/4, 0]			
O9					[3/8, 5/8, 1/2]			
O10					[3/8, 3/4, 0]			

Notes: The formula for the related mineral cahnrite, not in the table, is  $\text{Ca}_2\text{B}(\text{AsO}_4)(\text{OH})_4$ .

\* Only crystallographically non-equivalent directions are listed.

†  $U_{\text{cp}}$  calculated for the szenicsite of Stolz and Armbruster (1998), the antlerite of Vilminot et al. (2003), the deloryite of Pushcharovsky et al. (1996), and the flinkite of Moore (1967).

‡ Origin shifted [0, -1/4, -1/6] from the standard setting.

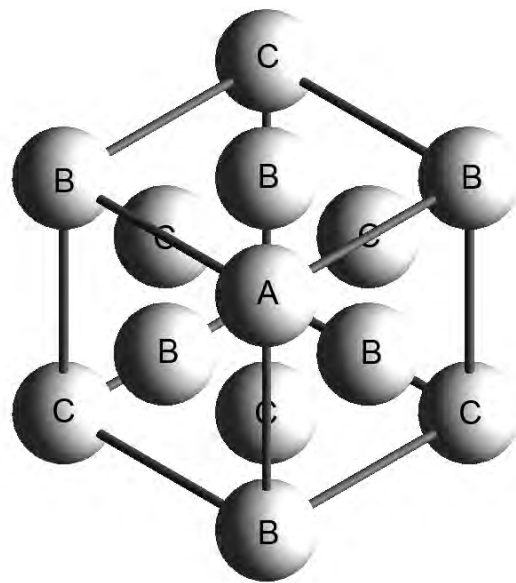


FIGURE 1. A face-centered cube looking down [111] at the closest-packed monolayers.

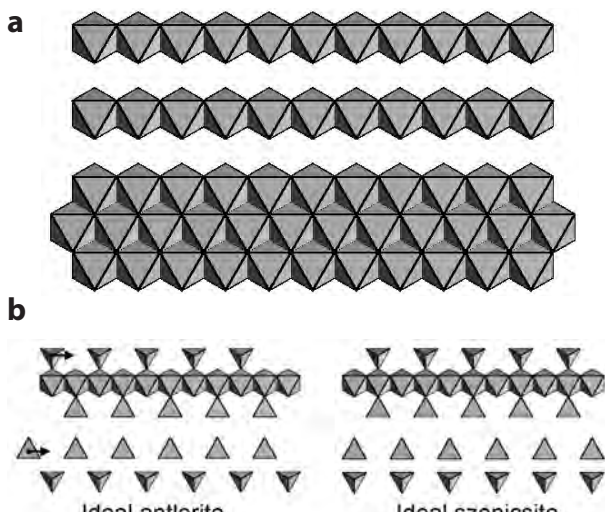


FIGURE 2. (a) The O-layers in ideal szenicsite and ideal antlerite are identical. A portion of the layer is illustrated here looking down [111] in szenicsite or the corresponding zone in antlerite, [101]. (b) A comparison of the T-layers in ideal antlerite (down [101]) and ideal szenicsite (down [110]). The layers are related to each other by a translation of half of the T cations to the nearest adjacent T site that does not change the apical direction of the T sites. All anions are fixed in place.

ideal szenicsite. Szenicsite is related to antlerite by a translation of half of the T cations to the nearest adjacent tetrahedra that preserve the apical orientation of the T sites and therefore do not fundamentally alter the way in which the layers are connected. In szenicsite, this is a translation parallel to **c** of  $c/2$  (**b** in antlerite). This translation involves only cations; the CCP oxygen arrangement remains fixed in place.

Hawthorne et al. (1989) state that staggering of the T sites in antlerite creates compensating distortions in the O triple chain to accommodate the mismatch in size with the relatively small sulfate T sites. Stoltz and Armbruster (1998) and Burns (1998) propose that the larger molybdate T sites in szenicsite do not create such a mismatch, removing the requirement that the T sites be offset from each other and therefore allowing for the slight structural difference seen in Figure 2b. In an ideal CP structure, the octahedral:tetrahedral volume ratio is exactly 4:1. In szenicsite (Stoltz and Armbruster 1998), the ratios for the nonequivalent O sites are 4.37:1, 4.40:1, and 4.15:1, while for antlerite (Vilminot et al. 2003) they are 7.17:1 and 7.44:1, consistent with the hypothesis of Stoltz and Armbruster (1998) and Burns (1998).

### Szenicsite and markascherite

Szenicsite and markascherite are dimorphic and closely related structurally. They have not been observed to transform from one to another, but szenicsite (Stoltz and Armbruster 1998) is approximately 1.5% denser than markascherite (4.279 vs. 4.216 g/cm<sup>3</sup>) and markascherite may transform to szenicsite with pressure. The structural relationship between markascherite and szenicsite is more complex than that of szenicsite and antlerite, and any set of cation translations that relates markascherite and szenicsite must include at least one translation between layers of polyhedra. However, it is obvious from visual inspection that zone [10̄5] in markascherite corresponds to zone [110] in szenicsite and [101] in antlerite.

Figure 3 is a cartoon of the T and O layers in ideal markascherite and ideal szenicsite viewed down [10̄5] and [110], respectively. A set of cation translations that relates the two structures is drawn on the figure. These translations can be

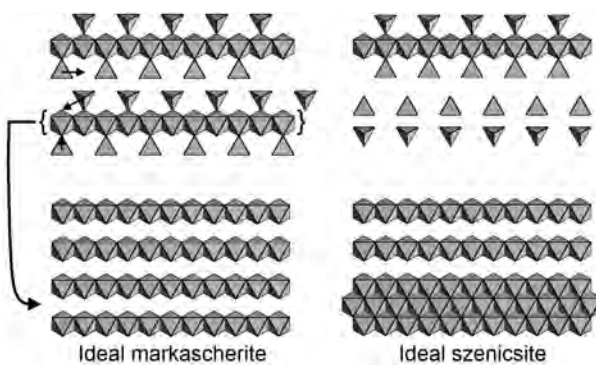


**FIGURE 3.** The relationship between markascherite and szenicsite. The T- and O-layers of ideal markascherite down [10̄5] and ideal szenicsite down [110] are illustrated along with arrows representing a set of cation translations that relate the two structures. Anions remain fixed in place.

interpreted as a simple possible transition pathway, but there are many others and the transition has not been observed. The set contains a translation that takes a cation from one layer to another: Cu1 in markascherite moves from the T layer to the nearest unoccupied O site in the adjacent O layer, resulting in the O layer of szenicsite. All of the T cation translations are within the T layer. One quarter of the T cations remain fixed in place, one quarter translate to the nearest tetrahedra that preserve the apical orientation of the T sites (one-half of a unit cell parallel to **b**), one quarter translate to the nearest tetrahedra that reverse the apical orientation, and one quarter move to the second-nearest tetrahedra that reverse the apical orientation.

### Szenicsite, antlerite, and markascherite

As illustrated above, zones [110], [101], and [10̄5] in szenicsite, antlerite, and markascherite, respectively, correspond to each other and provide orientations for visualizing their structural relationships. The small variations among these structures in this CP stacking direction, however, create changes in the other stacking directions that obfuscate the relatedness of the structures when viewed down these other zones, particularly in markascherite.

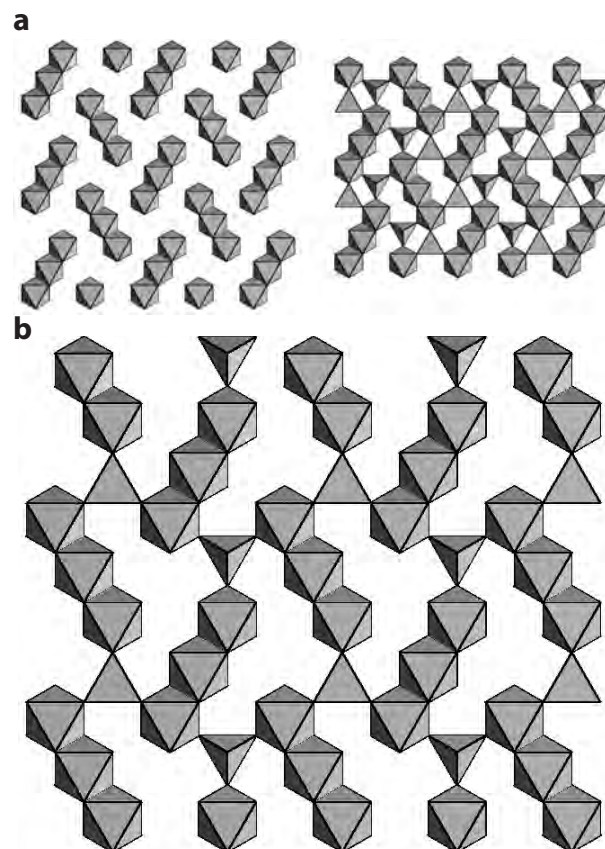


**FIGURE 4.** (a) The two layer types that alternate down [012] in szenicsite. The O arrangements in each layer type are identical, but all of the T sites are confined to just one of the layer types. (b) Ideal antlerite down [120]. This antlerite layer type has the same O distribution as the ideal szenicsite layers in (a), but each layer contains half of the T sites, resulting in only one layer type.

In szenicsite and antlerite, there is an obvious correspondence between the other two nonequivalent stacking directions, [012] and [120], respectively, as illustrated in Figure 4. Figure 4a is a cartoon of the two types of layers that alternate down [012] in ideal szenicsite. The distribution of O sites is identical in both layer types, but one of them contains all of the T sites, the other none. In ideal antlerite, each layer has the same arrangement of O sites as in ideal szenicsite, but only one-half of the T sites, resulting in only one layer type (Fig. 4b).

Markascherite is more complicated. There are two non-equivalent stacking directions in addition to [105]: [143] and [301]. There is only one layer type down [143], illustrated in Figure 5. Visual inspection reveals a resemblance to the layers stacked along [012] in szenicsite and [120] in antlerite, but it is different enough to result in a third nonequivalent stacking direction: [301]. There are four layer types stacked along [301], two O layer types interleaved with two T types. One of the O layer types is identical to the O layer along [105] (Fig. 3). Above this is a layer of evenly spaced isolated T sites pointing up [301]. This is followed by a brucite-type fully occupied O layer, and the sequence is completed by another layer of evenly spaced T sites, but pointing down [301]. These layers are illustrated in the subsection comparing markascherite and deloryite below.

Bond lengths and interatomic separations in ideal and observed equivalents with the same volume for a given mineral can often be compared to gain insight into which interatomic interactions are the driving force for distortion from ideal in the observed structure. In the case of szenicsite, antlerite, and markascherite, however, the presence of substantial hydrogen is likely contributing significantly to the distortion, making it difficult to draw reasonable inferences.

### Deloryite

Figure 6 is a visual comparison of the ideal CCP deloryite and the observed deloryite structure (Pushcharovsky et al. 1996) viewed down  $c^*$ . The two structures appear very similar, but

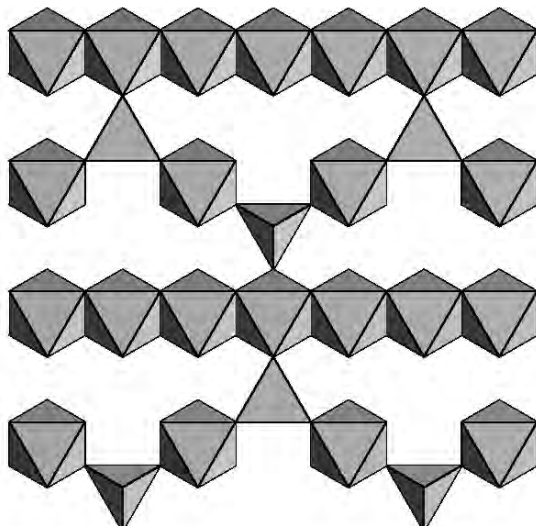


**FIGURE 5.** Markascherite is composed of these layers stacked along zone [143].

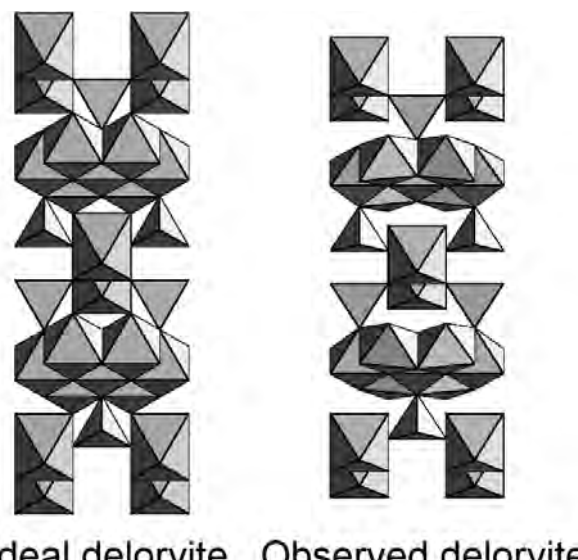


**FIGURE 6.** Ideal deloryite compared with observed deloryite (Pushcharovsky et al. 1996) looking down  $c^*$ .

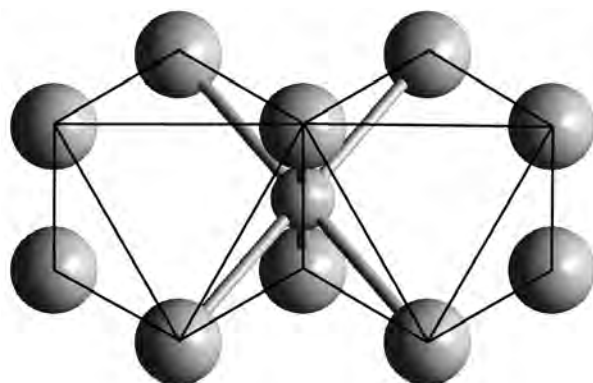


**FIGURE 7.** Cartoon looking down  $a^*$  showing that the uranium cation in ideal deloryite is placed on the midpoint of the shared edge of two unoccupied octahedra. The distorted O site created by this placement of the uranium cation has orientation or “tilt” (Papike et al. 1973) opposite that of the adjacent vacant octahedra.

Figure 7 shows that to reproduce the topology of the observed structure, the uranium atom in the ideal structure was not placed in an interstitial octahedral void in the CP arrangement of model anions, but at the midpoint of the shared edge of two such octahedral voids. This results in an unusual O site, better described as a square bipyramid, which is not a regular polyhedron. Faces in the monolayers (parallel to the plane of the page) of the square bipyramid share edges with faces in the monolayers of the adjacent vacant octahedra but point in opposite directions, i.e., the cation coordination bipyramid has “tilt” (Papike et al. 1973) opposite to that of the adjacent vacant octahedra. This point is illustrated in Figure 7, in which the triangular faces of the outlined vacant octahedra parallel to the page point south, while the (incompletely outlined) face of the uranium square

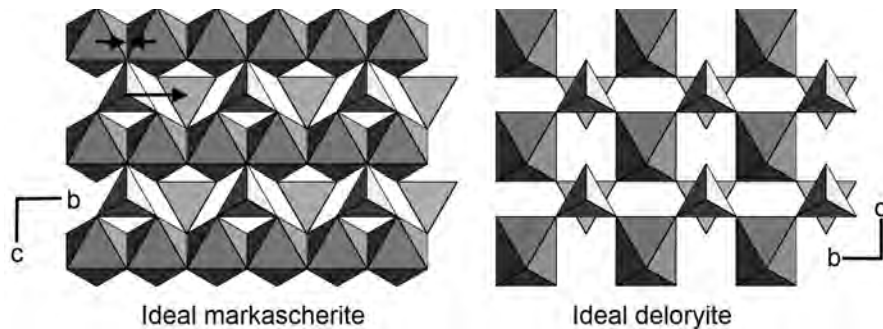


**FIGURE 8.** The relationship between markascherite and deloryite. Each pair of adjacent octahedrally coordinated copper cations is replaced by one uranium square bipyramidal at the midpoint of the line segment connecting the two copper atoms.

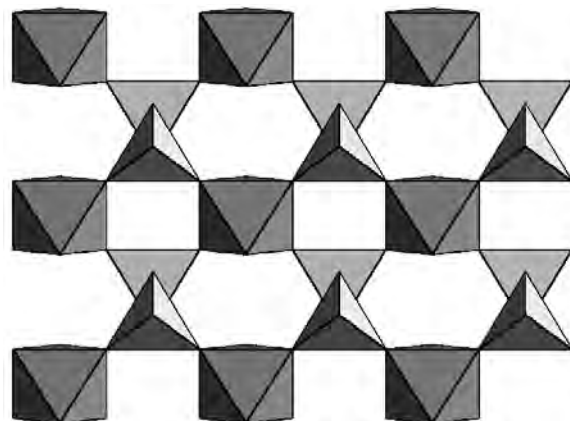


**FIGURE 9.** Observed deloryite (Pushcharovsky et al. 1996) viewed down  $a^*$ .

bipyramid points north.

The deloryite structure adopts this unusual topology (Fig. 8). The orbital configuration of electrons of  $U^{6+}$  makes this possible.  $U^{6+}$  in crystals typically coordinates to  $O^{2-}$  with two short, strong *trans* bonds about 1.8 Å long, forming a characteristic shortened axis and several equatorial bonds of length >2.2 Å. Examples include curite (Li and Burns 2000), umohoite (Krivovichev and Burns 2000), and masuyite (Burns and Hanchar 1999). In ideal deloryite, there are two U-O bonds of length 1.53 Å and four that are 2.66 Å long. The uranium site in deloryite is distorted from ideal so that bond lengths typical of  $U^{6+}$  cation polyhedra are formed: apical bond lengths of 1.80 Å and equatorial of 2.30 Å to achieve the best incident bond valence sums at  $U^{6+}$ . Figure 9 is a cartoon of the deloryite structure for comparison with Figure 8.

Table 1 contains values of the distortion parameter,  $U_{cp}$ , calculated for the CCP minerals analyzed in this discussion. The accommodation of the uranium atom is reflected in the high value of  $U_{cp}$  for deloryite, 0.66 Å<sup>2</sup>. By contrast,  $U_{cp}$  for the other three CCP minerals is less than 0.26 Å<sup>2</sup>.

#### Deloryite and markascherite

Deloryite (Pushcharovsky et al. 1996) and markascherite have very similar topologies (Yang et al. 2012). The corresponding stacking directions in deloryite and markascherite are [304] [1 0 12][184] and [301][105][143], respectively. Here, we will illustrate the structural relationship between the two minerals by

comparing the corresponding zones [304] in deloryite and [301] in markascherite. There are four different layer types stacked down these zones, two O layers interleaved with two T layers. One of the O layers in each mineral is a brucite-type layer. Figure 8 illustrates the relationship between the other three layers, which consist of an O layer sandwiched between two T layers. Each pair of adjacent copper O sites in markascherite is replaced by one uranium square bipyramidal in deloryite, centered on the midpoint of the line segment connecting the two copper atoms. Changing only this in the structure of markascherite would cause the T sites in one of the T layers to share edges with the resulting square bipyramidal sites, which would make the structure energetically unfavorable. Instead, these T cations are translated by  $b/2$  to the nearest tetrahedra in between the same monolayers that preserve the apical orientation of the T sites.

A result of this unusual geometry in deloryite is the presence of dangling oxygen atoms in both the T sites ( $O_4$ ) and square bipyramidal sites ( $O_1$ ). Pushcharovsky et al. (1996) did not locate the hydrogen atoms in deloryite. Their placement of hydroxyl groups would require extremely long hydrogen bonds were they to coordinate to the dangling O atoms, with the shortest  $O_1\text{-OH}$  distance being 3.14 Å and the shortest  $O_4\text{-OH}$  separation being 3.54 Å.

#### Flinkite

This subsection discusses two models for flinkite, an ideal closest-packed structure (ideal flinkite) and a modified model built from ideal monolayers that are not stacked in closest-packed fashion (hereafter referred to as model flinkite). Figure 10 is a visual comparison of ideal flinkite, observed flinkite (Moore 1967), and model flinkite viewed down  $c$ .

Ideal flinkite has a closest-packed arrangement of anions with the stacking sequence ABAC. Such a stacking sequence is necessary to reproduce the alternating “tilt” of the O layers. This alternation can be seen in Figure 10 in the triangles of the projection of the layers into the page. Layers alternate between up-pointing triangles and down-pointing triangles. For an in-depth discussion of octahedral tilt, see Papike et al. (1973). The stacking sequence ABAC does not have T sites that allow exact reproduction of the topology of observed flinkite (Moore 1967). The T sites in ABAC allow for one T site that exactly reproduces the topology of observed flinkite and a second nonequivalent T site that links to the O layers in a slightly different fashion. This forces a reduction in symmetry from  $Pnma$  to  $P2_1ma$ . This relationship between observed and ideal closest-packed flinkite

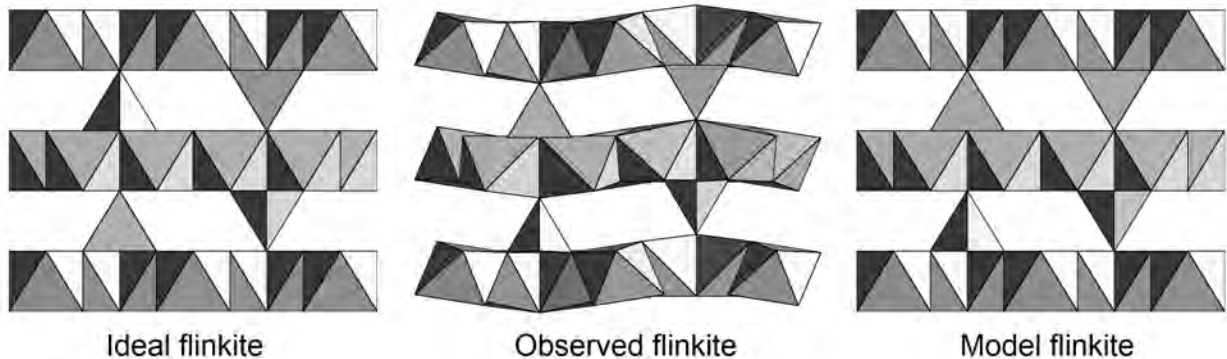


FIGURE 10. A comparison of ideal, observed (Moore 1967), and model flinkite looking down  $\mathbf{c}$ .

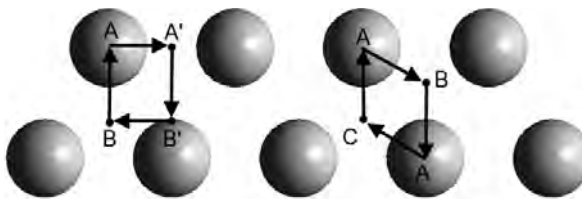


FIGURE 11. The difference in the oxygen packing between model flinkite with stacking sequence AA'B'B (**left**) and ideal flinkite with the stacking sequence ABAC (**right**). The translations between the A and B closest-packed monolayers and the A' and B' closest-packed monolayers in model flinkite create three-dimensional closest-packing on the scale of two monolayers, but the A to A' and B to B' translations do not.

is similar to that in protopyroxene, also based on the stacking sequence ABAC (Thompson and Downs 2003), which has the space group  $Pbcn$  at room conditions, but whose ideal equivalent has the space group  $P2_1cn$ . Protoproxene transforms under pressure to the  $P2_1cn$  structure (Yang et al. 1999), and the hypothetical ideal flinkite presented in this paper is our predicted high-pressure form of that mineral.

Model flinkite exactly reproduces the topology of observed flinkite but is no longer a closest-packed structure. Its stacking sequence can be described as AA'B'B, where the O layers A'B' and BA have closest-packed relationships, but AA' and BB' do not. Therefore, the O sites in model flinkite are regular, but the T sites are not. This does, however, allow all T sites to be equivalent, reproducing the space group of observed flinkite (Moore 1967). Figure 11 illustrates the difference between the stacking sequences of model and ideal flinkite.

The O layers of observed flinkite (Moore 1967) have an undulation. This means that the observed structure must necessarily be extremely distorted from both the ideal and model flinkites, which have perfectly flat O layers. The  $U_{cp}$  program was modified to handle stacking sequences ABAC and AA'B'B using a block of 672 anions. The value of  $U_{cp}$  between observed flinkite (Moore 1967) and ideal flinkite was  $1.08 \text{ \AA}^2$ , which reduced to  $0.88 \text{ \AA}^2$  when comparing observed and model flinkite.

A comparison of interatomic separations in observed (Moore 1967) and ideal flinkite may provide an explanation for the undulating character of the observed structure. The shortest  $M^{2+}$ - $T^{6+}$  distance in ideal flinkite is only  $2.59 \text{ \AA}$ . In natural flinkite,

shortest M-T distance is  $3.42 \text{ \AA}$ , 32% greater. In other words, the observed distortion from the ideal structure minimizes the repulsion between T and M. In model flinkite, the shortest M-T distance is  $3.35 \text{ \AA}$ , but the model T site has a physically impossible geometry that includes a planar angle of  $90^\circ$ , so the natural crystal must distort to make the T site more regular. The model T site can be thought of as a distorted Sommerville tetrahedron, as found in ideal body-centered cubic quartz (Sommerville 1923a, 1923b; Thompson and Downs 2010).

The various structures analyzed in this section have both very small (sulfate) and large (molybdate) T sites. Silicate T sites are intermediate in size between these two, and so size considered by itself would suggest that there might exist related silicate minerals. However, silicate T sites frequently polymerize, while all of the structures analyzed in this section have isolated T sites. This is because of the different charges the T cations carry. For instance, both sulfate and molybdate T sites are  $\text{TO}_4^{2-}$  groups, and a sulfate or molybdate T single chain would be electrically neutral. For an in-depth discussion of T polymerization in oxygen-based minerals, see Hawthorne (2006). For this reason, it would not be surprising to find related silicates with polymerized T sites.

A comparison of the arsenate flinkite with the silicates shattuckite and plancheite (Evans and Mrose 1977) illustrates these principles. Flinkite is an arsenate with a  $(\text{TO}_4)^3-$  group, intermediate in charge between the molybdate and the silicate T sites, but closer in size to a  $\text{SiO}_4$  group. Like the molybdates, it contains isolated T sites, but might more easily accommodate a silicate T substitution. In fact, the silicates shattuckite and plancheite are related structures. They are hydrous copper silicates composed of alternating layers of T and O sites with undulating structures similar to flinkite. Shattuckite has single chains of corner-sharing T sites and plancheite has double chain T polymers. Figure 12 shows the two structures viewed down  $\mathbf{c}$  for comparison with observed flinkite (Moore 1967), illustrated in Figure 10.

Based on the above discussion, we might expect to find or synthesize silicate structures related to markascherite and the other minerals of interest.

### Retzian

Retzian contains 8-coordinated yttrium, and should therefore be either non- $C_p$  or very distorted. Our investigation indicates that retzian is based on HCP with  $U_{cp} = 0.75 \text{ \AA}^2$ , a value indicating

extreme distortion. Figure 13 is a cartoon of one of two types of layers of polyhedra that occur in retzian, stacked in alternating fashion perpendicular to **c**. This layer is unusual in that it contains O chains with opposite tilts (Papike et al. 1973), a topology that

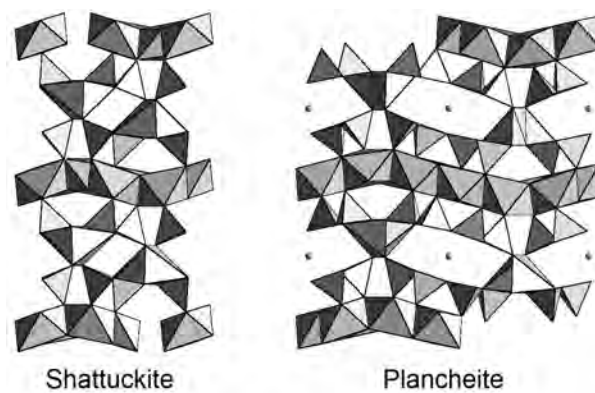


FIGURE 12. Shattuckite and plancheite (Evans and Mrose 1977) viewed down **c**.

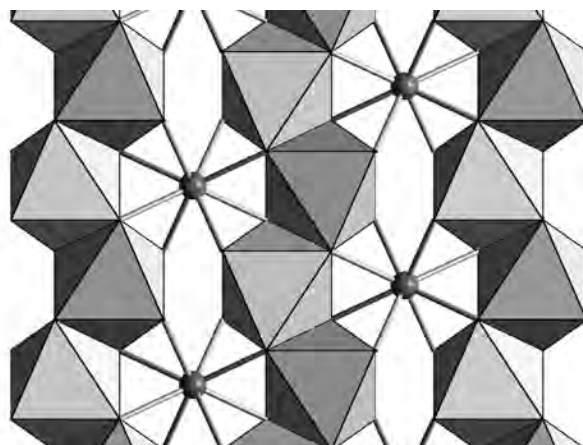


FIGURE 13. One of two types of layers of polyhedra found in retzian viewed down **c**. This layer is unusual in that it contains O chains of opposite tilt.

cannot occur in ideal CP.

Careful examination of the retzian monolayers reveals that they are distorted from CP in a systematic fashion, such that it is reasonable to define a new type of monolayer, the retzian-type or R-type. Figure 14 illustrates the relationship between an ideal CP monolayer and a perfect model R-type monolayer. In an R-type layer, one-half of the spheres are shifted  $r/\sqrt{3}$  parallel to **a** (of the retzian unit cell), where  $r$  is the model oxygen radius, and a much smaller amount parallel to **b**. This displacement of the spheres from CP creates novel topologies not seen in CP in the arrangements resulting from the regular stacking of R-type monolayers, including 8-coordinated sites, O chains in the same layer with different tilts (Papike et al. 1973), and T sites with edges parallel to the monolayers, instead of faces as in CP.

The retzian oxygen arrangement is based on the stacking sequence  $A_R B_R$ , and all of the distinctive features described above are observed in this mineral. Reproducing the retzian topology with an ideal HCP arrangement requires unusual deloryite-type O sites with Mn replacing U (not something seen in nature), and unrealistic T sites formed by the placement of cations off-center in O sites.

Table 1 contains crystallographic data for a hypothetical retzian built from  $A_R B_R$  stacking of model R-type layers in such a way that the coordination polyhedra of the O and T sites are regular, hereafter referred to as "model" retzian. Figure 15 places model R-type and "ideal" HCP retzian side-by-side for mutual comparison and comparison with observed retzian (Fig. 13) (Moore 1967). Crystallographic data for ideal retzian are also found in Table 1.

Model retzian is far from CP. Any CP arrangement of equal-size spheres fills 74.0% of space, but  $A_R B_R$  stacking of model R-type layers only fills 45.5% of space because the ratio of the volume of the O site to the volume of the T site in model retzian is  $6\sqrt{3}/\sqrt{2} = 7.35$ , but this ratio in any CP stacking sequence is 4. Therefore, the T site edge length defines the maximum sphere size, and the O site anions cannot be considered to be in contact. The ratio  $V_O/V_T$  in observed retzian is 6.40, much closer to model R-type than ideal HCP.

The distortion parameter for observed retzian increases from  $0.75 \text{ \AA}^2$  for ideal retzian to  $1.06 \text{ \AA}^2$  for model retzian, as calculated

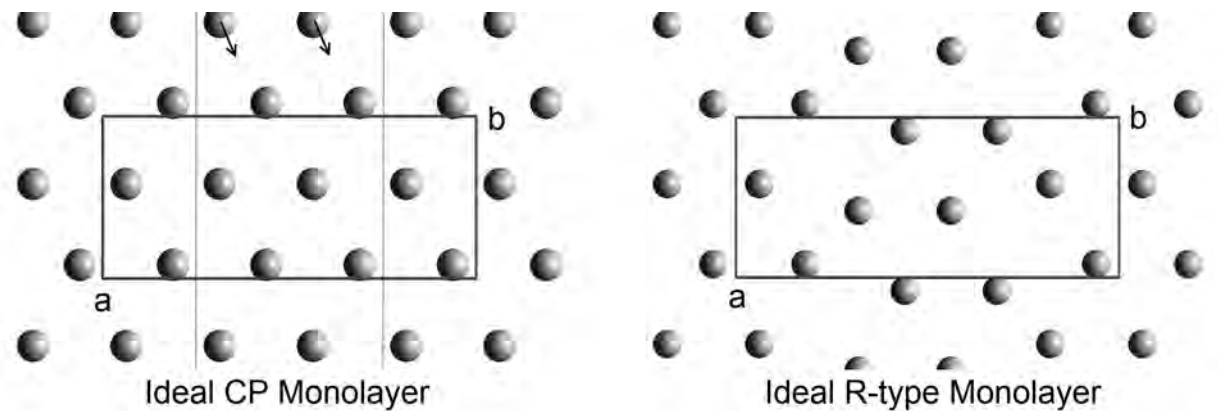
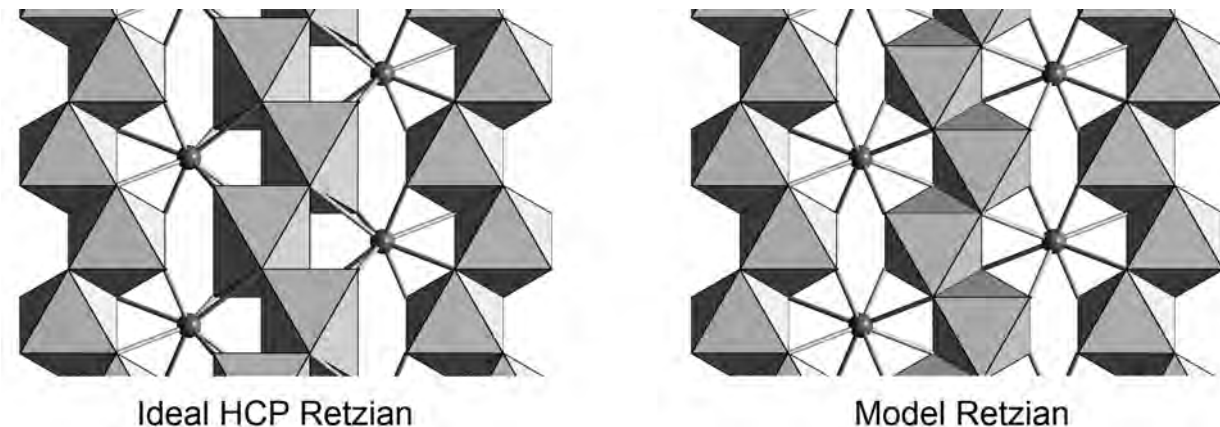
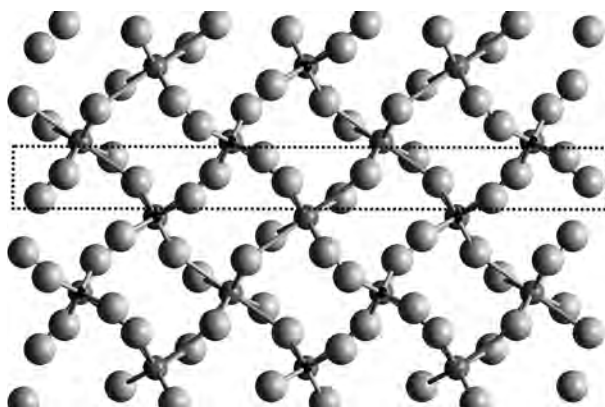


FIGURE 14. The relationship between ideal CP monolayers and a new type of monolayer, the retzian- or R-type.



**FIGURE 15.** A comparison of ideal HCP retzian with model retzian looking down  $\mathbf{c}$ . Contrast these with observed retzian (Fig. 13).



**FIGURE 16.** Cahnite viewed down  $\mathbf{c}$ . The dotted box isolates a monolayer, illustrating the distortion in three dimensions.

with our software using a block of 672 anions. This is because constraining both the tetrahedra and octahedra to be regular decreases the  $\mathbf{c}/\mathbf{a}$  axial ratio, and these parameters are sensitive to deviations from ideal axial ratios. Increasing the ratio by adding  $(\sqrt{2} - 2/\sqrt{3})r$  to  $\mathbf{c}$  decreases the distortion parameter to  $0.57 \text{ \AA}^2$ .

### Cahnite

Upon visual inspection, it is hard to imagine cahnite (Prewitt and Buerger 1961) as containing layers of O atoms. However, our software determined cahnite to be HCP with the stacking direction [110] and  $U_{cp} = 0.58$ , less than that of observed retzian. This is because the monolayers of cahnite are distorted in three dimensions, to the point where cahnite is hard to identify as a layered structure. Figure 16 is a cartoon of cahnite viewed down  $\mathbf{c}$ . The dotted box encapsulates a monolayer viewed edge-on to illustrate the three-dimensional distortion. As in the retzian example, an ideal HCP equivalent is not very meaningful. Continuing the analogy, cahnite can be constructed from CP monolayers altered in a fashion similar to that of Figure 14, but with twice as many staggered zones, each of half the width of those illustrated in Figure 14.

### ACKNOWLEDGMENTS

The authors thank Science Foundation Arizona for their support and reviewers Sergey Krivovichev and Frank Hawthorne for helping to improve our manuscript. We want to particularly acknowledge Dr. Hawthorne's above-and-beyond edit, and express our appreciation for the time it must have required.

### REFERENCES CITED

- Barlow, W. (1883) Probable nature of the internal symmetry of crystals. *Nature*, 29, 186–188, continued on 205–207.
- Bragg, S.L., Claringbull, G.F., and Taylor, W.H. (1965) *Crystal Structures of Minerals*. Cornell University Press, Ithaca, New York.
- Burns, P.C. (1998) The crystal structure of szenicsite,  $\text{Cu}_3\text{MoO}_4(\text{OH})_4$ . *Mineralogical Magazine*, 62, 461–469.
- Burns, P.C. and Hanchar, J.M. (1999) The structure of masuyite,  $\text{Pb}[(\text{UO}_2)_3\text{O}_3(\text{OH})_2](\text{H}_2\text{O})_x$ , and its relationship to protasite, *The Canadian Mineralogist*, 37, 1483–1491.
- Downs, R.T. (2003) Topology of the pyroxenes as a function of temperature, pressure, and composition as determined from the procrystal electron density. *American Mineralogist*, 88, 556–566.
- Evans, H.T. and Mrose, M.E. (1977) The crystal chemistry of the hydrous copper silicates, shattuckite and plancheite. *American Mineralogist*, 62, 491–502.
- Hales, T.C. (2000) Canniballs and honeycombs. *Notices of the American Mathematical Society*, 47, 440–449.
- Hawthorne, F.C. (2006) Landmark Papers: Structure Topology. *Mineralogical Society*, Middlesex.
- Hawthorne, F.C., Groat, L.A., and Eby, R.K. (1989) Antlerite,  $\text{Cu}_3\text{SO}_4(\text{OH})_4$ , a heteropolyhedral wallpaper structure. *Canadian Mineralogist*, 27, 205–209.
- Kepler, J. (1611) *Strena, Seu de Nive Sexangula, Francofurti ad Moenum*. Translated and reprinted as *The Six-Cornered Snowflake* (1966). Clarendon Press, Oxford.
- Krivovichev, S.V. and Burns, P.C. (2000) Crystal chemistry of the uranyl molybdates. I. The structure and formula of umohoite. *The Canadian Mineralogist*, 38, 717–726.
- Li, Y. and Burns, P.C. (2000) Investigations of crystal chemical variability in lead uranyl oxide hydrates. I. Curite. *The Canadian Mineralogist*, 38, 727–735.
- Lima-de-Faria (2012) The Close Packing in the Classification of Minerals. *European Journal of Mineralogy*, 24, 163–169.
- Moore, P.B. (1967) Crystal chemistry of the basic manganese arsenate minerals 1. The crystal structures of flinkite,  $\text{Mn}_{2+}^3\text{Mn}^{3+}(\text{OH})_4(\text{AsO}_4)$  and retzian,  $\text{Mn}_{2+}^3\text{Y}^{3+}(\text{OH})_4\text{AsO}_4$ . *American Mineralogist*, 52, 1603–1613.
- Papike, J.J., Prewitt, C.T., Sueno, S., and Cameron, M. (1973) Pyroxenes: comparisons of real and ideal structural topologies. *Zeitschrift für Kristallographie*, 138, 254–273.
- Pauling, L. (1940) *Nature of the Chemical Bond*. Cornell University Press, Ithaca, New York.
- Prewitt, C.T. and Buerger, M.J. (1961) The crystal structure of cahnite,  $\text{Ca}_2\text{BaSi}_4(\text{OH})_4$ . *American Mineralogist*, 46, 1077–1085.
- Pushcharovsky, D.Y., Rastsvetaeva, R.K., and Sarp, H. (1996) Crystal structure of delortyite,  $\text{Cu}_4(\text{UO}_2)[\text{Mo}_2\text{O}_8](\text{OH})_6$ . *Journal of Alloys and Compounds*, 239, 23–26.
- Sommerville, D.M.Y. (1923a) Division of space by congruent triangles and tetrahedra. *Proceedings of the Royal Society of Edinburgh*, 43, 85–116.

- (1923b) Space filling tetrahedra in Euclidean space. Proceedings of the Edinburgh Mathematical Society, 41, 49–57.
- Stoltz, J. and Armbruster, T. (1998) X-ray single-crystal structure refinement of szenicsite,  $\text{Cu}_3\text{MoO}_4(\text{OH})_4$ , and its relation to the structure of antlerite,  $\text{Cu}_3\text{SO}_4(\text{OH})_4$ . Neues Jahrbuch für Mineralogie Monatshefte, 278–288.
- Tait, K.T., Barkley, M.C., Thompson, R.M., Origlieri, M.J., Evans, S.H., Prewitt, C.T., and Yang, H. (2011) Bobdownsite, A new mineral species from Big Fish River, Yukon, Canada, and its structural relationship with whitlockite-type compounds. The Canadian Mineralogist, 49, 1065–1078.
- Thompson, R.M. and Downs, R.T. (2001) Quantifying distortion from ideal closest-packing in a crystal structure with analysis and application. Acta Crystallographica B, 57, 119–127.
- (2003) Model pyroxenes I: ideal pyroxene topologies. American Mineralogist, 88, 653–666.
- (2008) The crystal structure of diopside at pressure to 10 GPa. American Mineralogist, 93, 177–186.
- (2010) Packing systematics of the silica polymorphs: The role played by oxygen-oxygen nonbonded interactions in the compression of quartz. American Mineralogist, 95, 104–111.
- Vilminot, S., Richard-Plouet, M., Andre, G., Swierczynski, D., Guillot, M., Bou-  
ree-Vigneron, F., and Drillon, M. (2003) Magnetic structure and properties of  $\text{Cu}_3(\text{OH})_4\text{SO}_4$  made of triple chains of spins  $s = \frac{1}{2}$ . Journal of Solid State Chemistry, 170, 255–264.
- Yang, H., Finger, L.W., Conrad, P.G., Prewitt, C.T., and Hazen, R.M. (1999) A new pyroxene structure at high pressure: single-crystal X-ray and Raman study of the  $Pbcn-P2_{1}cn$  phase transition in protopyroxene. American Mineralogist, 84, 245–256.
- Yang, H., Jenkins, R.A., Thompson, R.M., Downs, R.T., Evans, S.H., and Bloch, E.M. (2012) Markascherite,  $\text{Cu}_3(\text{MoO}_4)(\text{OH})_4$ , a new mineral species polymorphic with szenicsite, from Copper Creek, Pinal County, Arizona, U.S.A. American Mineralogist, 97, 197–202.

MANUSCRIPT RECEIVED FEBRUARY 8, 2012

MANUSCRIPT ACCEPTED JULY 9, 2012

MANUSCRIPT HANDLED BY LARS EHM